# Comparison of molecular dynamics simulations with triple layer and modified Gouy-Chapman models in a 0.1 M NaCl-montmorillonite system

Christophe Tournassat, Yves Chapron, Philippe Leroy, Mohamed Bizi, Faïza Boulahya

# Comparison of molecular dynamics simulations with Triple Layer and modified Gouy-Chapman models in a 0.1 M NaCl - montmorillonite system

Christophe Tournassat[1*], Yves Chapron[2], Philippe Leroy[1], Mohamed Bizi[1], Faïza Boulahya[1]

[1] BRGM, French Geological Survey, Orléans, France

[2] AIED, La Terrasse, France

[*]Corresponding author and mailing address:

Christophe Tournassat

BRGM

Environment and Process Division (EPI/MIS)

3 Avenue Claude Guillemin

45060 Orléans Cedex 2, France

E-mail: c.tournassat@brgm.fr

Tel: +33 (0)2 38 64 47 44

Fax: +33 (0)2 38 64 30 62

**Abstract**

Molecular dynamics (MD) simulations of a montmorillonite / water interface at the pore scale were carried out at 0.1 mol $L^{-1}$ NaCl concentration in order to constrain cation, anion and water distribution and mobility influenced by the mineral surface. MD results enabled anion exclusion and cation condensation at the surface to be quantified. MD derived values could then be compared with macroscopic model results obtained from the modified Gouy-Chapman (MGC) theory. While the Na concentration profile is well reproduced in the diffuse layer, anion exclusion is overestimated by the MGC theory in our experimental conditions. We also showed that MD simulations can be used to constrain Basic Stern model parameters or, in combination with zeta potential measurements, can be used to constrain triple layer model (TLM) parameters by providing suitable values for the capacitance values. Na sorption intrinsic equilibrium constant values for clay basal surfaces are given accordingly.

Keywords: clay, molecular dynamics, Gouy-Chapman, Basic Stern model, triple layer model, cation exchange, diffusion.

## 1. Introduction

The study of the electrochemical properties of clay / water interfaces is of primary importance in soil and environmental chemistry: clay surface / ion interactions greatly influence not just soil aggregation and nutrient availability for plants but also contaminant mobility [1]. For the latter reason, the electrochemical properties of clay / water interfaces have been intensively studied to characterize the migration of ionic species around waste repositories (e.g. [2-5]). Clay formations are being considered to investigate the disposal of high-level radioactive waste in various European countries and have been the target of many studies over the past decade to determine their capacity to act as a host rock for high-level, long lived nuclear waste. The retention properties of these clay rocks are related to their very low permeability, high structural charge and surface area associated with the clay minerals. A comprehensive study of their surface properties and particularly of the ionic composition and mobility is necessary to assess the safety of the geologic disposal. Among the variety of minerals composing argillites and bentonites, montmorillonites are important because they have a large surface area for interaction with water molecules and dissolved ions. The characterization of the montmorillonite / water interface using electrostatic surface complexation models such as the double (DLM) or triple layer model (TLM) has already been the subject of many papers (e.g. [1, 6-9]). These macroscopic models are very useful for determining the ionic composition, i.e. cation condensation and anion exclusion at the interface. The DLM and TLM use the Gouy-Chapman model [10, 11] to describe the electrostatic interactions between the excess of charges of the clay minerals and the counter- and co-ions, the resulting electrostatic electrical field obeying the Poisson equation. The Poisson-Boltzmann equation can be further coupled with the

Navier-Stokes equation (hydrodynamics) to characterize, for example, the influence of the electrical charges on ionic and water fluxes [6, 12].

However, some assumptions of the model may not be valid. For instance, the theory assumes that the ions are point charges embedded in a continuum of constant dielectric that are distributed according to Boltzmann statistics. This assumption may not be valid if, for example, the water content is very low [5] or at high surface charge and ionic strength, because the size of the solvent molecules and the hydrated counter-ions cannot be neglected [13]. Another problem concerns the interpretation of the TLM parameters and their relation to the structural, physical and chemical properties of the interface [14].

Unlike macroscopic models, microscopic simulations such as molecular dynamics (MD) or Monte Carlo (MC) simulations explicitly take into account every atom in the system. These simulations have the advantage of giving accurate representations of the water, cation and anion concentration profiles and diffusivities ([5, 15-21]). Nevertheless, microscopic simulations require considerable computational effort and are thus time consuming, restricting molecular modelling to short length and time scales. The small size of the simulated systems also makes it necessary to consider a model composition and structure that are idealized compared to the real system. Microscopic simulations do not provide direct access to transport properties at the macroscopic scale.

The idea presented in this paper is to check the validity of the macroscopic electrostatic models by using molecular dynamics calculations in the case of a dilute NaCl - montmorillonite system. Recently, Rotenberg et al. [22] used MD and MC to access the range of validity of macroscopic equations (Navier-Stokes and Poisson-Boltzmann) in clayey media containing montmorillonite. However, these authors do not consider the existence of the compact Stern layer at the interface. As far as we know, there has been

no attempt yet to use MD as a benchmark to constrain TLM parameters at the montmorillonite / water interface and to validate ionic composition derived from the macroscopic electrostatic descriptions. Molecular dynamics calculations were therefore performed in order to provide an exact representation of the water, cation and anion concentration profiles in a solution influenced by a smectite surface at solute concentrations representative of the porewater in natural clayey media (I ~ 0.1, [23]). We restricted ourselves to the case of a binary symmetric monovalent electrolyte (NaCl) where we hoped to find good correlation between MD and MGC / TLM models.

## 2. Materials and methods

### *2.1 Geometry of the MD system*

A periodical 3D system was considered with two smectite TOT layers inserted between two water boxes. The clay structure was built based on a mica structure [24]. Octahedral charge of the clay was ensured by random substitutions of $Al^{3+}$ by $Mg^{2+}$ using an exclusion rule so that two substitutions could not occur on two adjacent sites. The interlayer water structure was a two water layer structure in agreement with XRD results on water saturated compacted Na-smectite at montmorillonite partial dry density between 1.6 and 1.8 $kg/dm^3$ [25]. An interlayer water specific mass of ~0.24 $kg_{water}/kg_{clay}$ [26, 27] was considered together with a d-spacing of 15.7 Å in agreement with XRD measurements. The periodic conditions of the systems were: $a = b = 52.138$ Å with $\alpha = 120°$ $c = 169.5$ Å for a total of ~40,000 atoms of which ~ 11,500 water molecules (~34,500 atoms). The Mg for Al substitutions (Mg + Al = 200, Mg = 32 for one layer and 36 for the other) result in a mean layer charge of 0.116 C $m^{-2}$, representative of a montmorillonite. No significant difference was observed between the two surfaces having slightly different charges (0.109 C $m^{-2}$ and 0.123 C $m^{-2}$) with

regards to water and ion distribution and results at both interfaces were averaged. Charge deficits were equilibrated by adding $Na^+$ surface cations. Half of the total charge was compensated by cations in the interlayer. The other half was randomly put at a distance of 3.2 ± 1 Å of the most external oxygen atoms of the structure. In the following, the term "charge deficit of the clay structure" will refer to the charge deficit that is not compensated by interlayer cations. In addition, 10 $Na^+$ and 10 $Cl^-$ ions were inserted in both the upper and lower water boxes leading to a total concentration (and ionic strength) of ~0.10 mol $L^{-1}$, corresponding to (i) the lowest concentration limit for statistical analysis of anion distribution profiles from molecular dynamics results (with regard to the computer capabilities devoted to the project) and (ii) to an ionic strength representative of natural conditions in clayey media (e.g. [23, 28]).

*2.2 Clay and water force fields*

In the proposed simulations, the CLAYFF force field [29] describes external and internal clay mineral surface / water + ion interactions. The force field used to describe the non-bonded interaction energy terms between clay atoms, water atoms and ions consists of pairwise interactions. The interaction between two atoms is represented by a direct electrostatic (Coulomb) contribution and a Lennard-Jones potential to account for short-range repulsion and long-range dispersion forces. In the simple point charge (SPC) water model, every water molecule has three charged sites centred on each of the $H_2O$ atoms [30, 31]. Flexible water molecule parameters have been introduced into the SPC water model of CLAYFF by Cygan et al. [29] using bond stretch and bond angle terms with expressions determined by Teleman et al. [32]. Although CLAYFF enables the modelling of a flexible clay network, we considered a rigid clay network in order to simplify post-processing of data. The atoms in the clay structure (Si, Al, Mg, O and H

atoms) were fixed but cations and water in the interlayer and on external surfaces were allowed to move, similarly to previous studies (e.g. [15, 17, 33, 34]).

Moreover, additional simulations using SPC/E force field charge parameters for water [30] were run in order to better scale the diffusion coefficients of solute species (models using SPC force field overestimate the water self diffusion coefficient. The SPC/E model corrects this problem with a slightly different charge distribution on the charged sites of the water molecule).

*2.3 Numerical methods*

Initial structure and coordinate files were prepared using XPLOR-NIH [35, 36]. NAMD [37] was used to perform molecular dynamics simulations in the NVT ensemble (constant number of particles, volume and temperature). All calculations were performed at 298 K and zero applied pressure. The coulombic interactions were calculated using the particle mesh Ewald summation method. An equilibration period of 1 ns was applied to the systems before the data were interpreted over a 5 ns period.

*2.4 Post-processing of MD results*

Trajectories of atoms were sampled every 0.1 ps. Wordom [38] was used to extract coordinate files as a function of time. Mean concentration profiles of $H_2O$ (the oxygen atom position taken as the centre of mass of the molecule), Na and Cl were calculated from coordinate files (with 0.5 Å and 0.01 Å resolutions) together with radial distribution function of water around Na and Cl as a function of clay surface distance. Previous studies (e.g. [17, 39]) have shown that dynamic properties of water and ions vary with the distance from the clay surface. As a consequence, diffusion coefficients parallel to the *ab* plane were calculated with the approach developed by Liu et al. for

confined fluids and interfaces [40]. Dynamic properties were averaged within different layers of water at the clay surface, the boundaries of which were defined from density profile oscillations.

*2.5 Zeta potential measurements on natural montmorillonite particles*

Zeta potential measurements were performed on the <2µm fraction of MX-80 bentonite. The whole extraction procedure is reported in [41]. The same material was used. The CEC (cation exchange capacity) of MX80 material was determined by cation extraction using the cobalt hexamine method (modified after [42]) and led to a value of 0.65 ± 0.04 $mol_c$/kg. Taking into account the impurities content (~23%, [41]), the cation exchange capacity of the clay fraction is 0.84 $mol_c$ $kg^{-1}$, corresponding to a surface charge of approximately -0.11 C $m^{-2}$.

Electrophoretic mobility ($\mu_e$; in $m^2$ $s^{-1}$ $V^{-1}$) measurements were performed on a ZetaSizer IV (Malvern Instruments Ltd) in optical configuration. Zeta potentials ($\zeta$ in V) were calculated using the Smoluchowski approximation:

$$\zeta = \frac{\mu_e \eta}{\varepsilon} \quad (1)$$

where $\varepsilon$ is the permittivity of water (in F $m^{-1}$) and $\eta$ is the viscosity of water (in Pa s).

Analyzed clay suspensions were prepared at a solid to water content of 0.1 g $L^{-1}$ in Milli-Q water. Each suspension was homogenised and dispersed by mechanical stirring and further ultrasonic treatment (2 minutes at 40 kHz). Ionic strength was then increased before measurements by adding analytical grade NaCl salt for a final concentration of 0.12 mol $L^{-1}$.

## 3. Na sorption and diffuse ion swarm modelling

### *3.1 MGC theory*

The modified Gouy-Chapman theory enables a quantitative description of the anion and cation concentration profiles in the vicinity of a uniformly charged (with surface charge density, $\sigma$ in $m^{-2}$) and flat surface and assuming that (i) the water is a uniform continuum characterized by its dielectric permittivity ($\varepsilon=\varepsilon_0\times\varepsilon_w$ where $\varepsilon_0$ is the permittivity of vacuum, $8.85419\times10^{-12}$ F $m^{-1}$, and $\varepsilon_w$ is the relative permittivity of water, 78.3 at 298 K) and (ii) that the potential of the mean force is proportional to $\psi(x)$, the mean electrostatic potential (in V), at a distance $x$ perpendicular to the surface [43]. Under these conditions, $Na^+$ and $Cl^-$ concentration profiles ($c_i$ with $i$ = $Na^+$ or $Cl^-$) in the investigated system can be calculated according to the following equation system (with $x > a$):

$$\frac{F\psi(x)}{RT} = 4\times\operatorname{arctanh}\left[\tanh\left(\frac{F\psi(a)}{4RT}\right)\times\exp\left(-\kappa(x-a)\right)\right] \quad (2)$$

$$c_i(x) = c_{i0}\times\exp\left(-Z_i\times\frac{F\psi(x)}{RT}\right) \quad (3)$$

$$\kappa = \sqrt{\frac{2F^2 1000 c_{i0}}{\varepsilon RT}} \quad (4)$$

$$\frac{F\psi(a)}{RT} = -2\times\operatorname{arcsinh}\left(\frac{F^2|\sigma|}{2\kappa\varepsilon RTN_A}\right) \quad (5)$$

Where $F$ is the Faraday constant (96485 C $mol^{-1}$), $R$ the gas constant (8.314 J $mol^{-1}$ $K^{-1}$), $T$ the temperature (K), $N_A$ the Avogadro number (6.022 $10^{23}$ $mol^{-1}$), $a$ the distance of closest approach to the surface of ions (m), $\kappa$ the inverse of the Debye length ($m^{-1}$), $Z_i$ the charge of ion $i$ (in our case +1/-1) and $c_{i0}$ the concentration at "infinite" distance from the surface (in mol $dm^{-3}$).

*3.2 Basic Stern and TLM theory*

The TLM used for describing the system is very similar to that depicted in Leroy et al. [44]. The charged clay surface is counterbalanced by cations adsorbed at the mineral surface (at 0-plane, see Figure 1), in the compact layer (at β-plane, see Figure 1) and in the diffuse layer together with anion exclusion from the Stern layer (complete exclusion) and the diffuse layer (anion concentration decreases exponentially as a function of the d-plane vicinity). Cations compensating the deficit of charge layer undergo the reaction:

$$XNa \Leftrightarrow X^- + Na^+ \qquad K_{Na\_0} \text{ (at 0-plane)} \tag{6}$$

$$X^{-\cdots}Na^+ \Leftrightarrow X^- + Na^+ \qquad K_{Na\_\beta} \text{ (at β-plane)} \tag{7}$$

where $X^-$ represents a charged site at the clay surface and $K_{Na}$ is the equilibrium constant (mol $dm^{-3}$) according to:

$$K_{Na\_0} = \frac{c_{X^-} a_{Na\,0}}{c_{XNa}} \exp\left(-\frac{F\psi_0}{RT}\right) = \frac{Q_0 + Q_\beta}{Q_{struct} - Q_0} a_{Na\,0} \exp\left(-\frac{F\psi_0}{RT}\right) \tag{8}$$

$$K_{Na\_\beta} = \frac{c_{X^-} a_{Na\,0}}{c_{X\cdots Na}} \exp\left(-\frac{F\psi_\beta}{RT}\right) = \left(-\frac{Q_0}{Q_\beta} - 1\right) a_{Na\,0} \exp\left(-\frac{F\psi_\beta}{RT}\right) \tag{9}$$

where $c_i$ denotes concentration, $a_i$ denotes activity (calculated using the Davies equation), $\psi_0$ and $\psi_\beta$ are the mean electric potential at the 0 and β-plane (V), $Q_0$ and $Q_\beta$ are the corresponding surface charge densities (C $m^{-2}$), and $Q_{struct}$ is the structural surface charge density (-0.116 C $m^{-2}$).

Under these conditions, the following equations and parameters describe the system:

$$Q_{struct} = \frac{F\sigma}{N_A} \tag{10}$$

$$Q_d = -2\sqrt{2\varepsilon RTc_{i0}} \times \sinh\left(\frac{F\psi_d}{2RT}\right) \tag{11}$$

$$Q_\beta = -Q_0 - Q_d \tag{12}$$

$$\psi_\beta = \psi_d - \frac{Q_d}{C_2} \tag{13}$$

$$\psi_0 = \frac{Q_0}{C_1} + \psi_\beta \tag{14}$$

where $Q_d$ is the surface charge density in the diffuse layer (C $m^{-2}$), and $\psi_d$ is the electrostatic potential at the d- plane (V). The parameters $C_1$ and $C_2$ represent the constant capacitances of the two condensers corresponding to the inner and outer part of the Stern layer (in F $m^{-2}$). The diffuse layer composition can be calculated as a function of $x$, the distance from the d-plane, by setting $a$ = 0 and by replacing $\psi(a)$ by $\psi_d$ in

equations 2 to 5.

The Triple Layer model can be further transformed into the Basic Stern model by setting $C_2$ equal to infinity (corresponding to the absence of the outer part of the Stern layer, i.e. $x_2 = 0$).

## 4. Results and discussion

### *4.1 Molecular dynamics results*

Figure 2 shows that there is very little influence of water force field (SPC or SPCE) on the MD results for water density and $Na^+$ concentration profiles. For $Cl^-$ profile, the scatter of the data (due to the low $Cl^-$ concentration, 0.1 mol $L^{-1}$ and consequently poor statistics) seems to indicate that this difference could also be due to an insufficient simulation time. For the following analysis, we decided to merge the SPC and SPCE results in order to smooth this effect.

The water density profile was computed based on the position of the oxygen atom of the water molecule. Water was found to be strongly structured in the first 5 Å from the most external oxygen atom of the clay, showing density oscillations up to a distance of 10 Å. The water maximum density depends on the spatial analysis resolution. At a 0.5 Å resolution, the first sorbed layer of water has a maximum density of about 2.0 kg $dm^{-3}$, a value below that observed in the interlayer space (~2.8 kg $dm^{-3}$). At finer resolution (0.01 Å), this difference in maximum density almost vanished with values of 3.1 and 3.4 kg $dm^{-3}$ for the first sorbed layer of water and interlayer water respectively. This water maximum density is comparable to the density calculated by MD on other phyllosilicate mineral surfaces such as muscovite or talc [45] or clays [17, 46]. The maximum density peak position is at ~2.65Å from the coordinate of the most external oxygen atoms of the clay structure and corresponds therefore to slightly less than the

distance of one oxygen ion radius ($r_O$=1.4 Å) plus one water molecule radius ($r_{H2O}$~1.5 Å). The mean water density in the structured water can be calculated with the density profile and is equal to the bulk water density when integrating the two first oscillations from the clay surface coordinates (density difference less than 2%).

In the following, the clay surface refers to the coordinate of the centre of the most external oxygen atoms plus the distance of one oxygen ion radius (with this convention, the water density peak is located at ~1.25 Å from the clay surface). The sodium concentration profile shows a "plane" of adsorbed sodium near to the surface and then the presence of a diffuse layer. The "plane" of sorbed Na is located at 2.8 Å from the surface with a start of the concentration peak at 1.8-1.9 Å, in agreement with the distance of closest approach of $Na^+$ usually considered in the MGC model (3.74/2 = 1.87 Å). In the sorption plane, Na is mostly present as outer-sphere complexes and keeps its 5-6 coordination waters as shown by the radial distribution function of water around Na cations (Figure 3). A very minor part of Na (~6% of the surface charge) is engaged in sorption sites where the Na hydration shell has lost up to 3 water molecules.

The results of the simulation show a decreasing $Cl^-$ concentration as $Cl^-$ approaches the clay surface (Figure 2). Due to anion repulsion from the clay surface, the $Cl^-$ concentration increases by 0.02 mol $L^{-1}$ in the water far from the surface (~0.12 mol $L^{-1}$) as compared to the initial $Cl^-$ mean concentration (0.1 mol $L^{-1}$). The closest distance of Cl approach is very near the clay surface and ends roughly when the plane of sorbed $Na^+$ is met. $Cl^-$ concentration becomes equal to $Na^+$ concentration (concentration difference less than 10%) at about 25 Å from the clay surface.

Ion and water diffusion coefficients were computed using the methods of [40], applied to six distinct zones parallel to the clay surface: I: interlayer, II: Na inner-sphere and first peak of water density, III: main peak of sodium concentration, IV: second

oscillation of water density and start of the diffuse layer, V: end of the diffuse layer and VI: bulk. These zones can be seen in Figure 4. Only diffusion coefficients parallel to the surface ($D_s$) were computed. The calculated bulk water diffusion coefficients ($D_{0w}$) are 2.8 and 4.3 $10^{-9}$ $m^2$ $s^{-1}$ for the SPC/E and SPC force field respectively (measured diffusion coefficient in water is 2.4 $10^{-9}$ $m^2$ $s^{-1}$ at 25°C). While the SPC derived diffusion coefficient is in agreement with the value reported in the literature with this force field model (4.3 $10^{-9}$ $m^2$ $s^{-1}$, [30]), our SPC/E simulations led to a slightly higher value than that usually reported (2.5 $10^{-9}$ $m^2$ $s^{-1}$). As a consequence, the calculated values must be scaled to the real value in order to be interpreted, e.g. in terms of relative water viscosity in the different compartments. Diffusion coefficients were scaled to the value obtained in the bulk water ($D_{si}/D_{0i}$ where $i$ = water, Na or Cl) for further comparisons. Once scaled, the changes in the diffusion coefficient as a function of the clay surface distance remains similar whatever the force field (Table 1), showing a decrease in water and sodium mobility as they approach the surface, in agreement with previously reported MD results [17]. Our results are also in agreement with results from Lockhart [47] considering a minimum $D_{sNa}/D_{0Na}$ value of 1/3 in the Stern layer of a montmorillonite gel using the Stokes-Einstein relationship and considering the ratio of fluid viscosities in the Stern and diffuse layers.

*4.2 Comparison of MD results with MGC and TL models*

For reasons of simplicity, in the following the abscissa $x$=0 (or clay surface) corresponds to the position at one oxygen ion radius from the centre of the most external oxygen atoms in the clay (i.e. top of surface oxygen atoms).

*4.2.1 Anion exclusion and cation condensation*

Figure 5 shows the Na and Cl concentration profile obtained from equations (2) to (5) and their comparison with profiles obtained from MD calculations (the mean of the simulation performed with SPC and SPC/E force fields). A 0.116 mol $L^{-1}$ NaCl background concentration ($c_0$) was chosen according to the mean concentration of Na and Cl on the last 20 Å of the MD profiles. The surface charge was taken as equal to that exhibited by the clay surface in the MD simulation (-0.116 C $m^{-2}$). A distance of closest approach of $a$ = 1.84 Å was considered for $Cl^-$ and $Na^+$, representative of a mean hydrated radius for these two ionic species [43].

There is good overall agreement between the MGC model predictions and our MD results. In particular, the good agreement of sodium concentration profiles in the diffuse swarm for $x$ > 5 Å may be noted. As expected, the MGC model is not able to reproduce exactly the position of the Na condensation zone. Cation condensation at the interface can be quantified by the following $\varphi(x)$ function [43]:

$$\varphi(x) = -\frac{N_A}{\sigma}\int_a^x \left(c_{\mathrm{Na}}(x') - c_0\right)dx' \qquad (15)$$

where $a$ is the ions' distance of minimum approach (1.84 Å) and $c_{\mathrm{Na}}(x)$ represents the concentration of sodium at distance $x$ from the surface.

This function can be calculated for both MD and MGC results. Figure 6 shows that cation condensation is shifted to higher $x$ values and underestimated by the MGC model. However, the extent of underestimation is low and the two curves could be almost superposed when considering that the small part of Na that undergoes a loss of water hydration becomes part of the surface charge term (then decreasing $\sigma$, Figure 6).

The MGC chloride concentration profile shows higher anion exclusion than the MD

simulations. This difference can be appreciated more quantitatively by considering the anion exclusion distance given by the MGC model [48]:

$$d_{ex} = \lim_{x\to\infty} \int_a^x \left(1 - \frac{c_{\mathrm{Cl}}(x')}{c_0}\right) dx' + a = \frac{2}{\kappa}\left(1 - \exp\left[-\frac{F|\psi(a)|}{2RT}\right]\right) + a \qquad (16)$$

The integral expression can also be evaluated with the MD simulation results as a function of x:

$$d_{ex} = \lim_{x\to\infty}\left(Ex_{DM}(x)\right) \qquad (17)$$

With

$$Ex_{DM}(x) = \Delta x \times \sum_{i=0}^{x/\Delta x}\left(1 - \frac{c_{\mathrm{Cl}}(i\times\Delta x)}{c_0}\right) \qquad (18)$$

where $\Delta x$ is the resolution of the molecular dynamics trajectory analysis.

Because the determination of $c_0$ from molecular dynamics results is subject to non-negligible uncertainty (due to statistical reasons), Figure 7 shows the $Ex_{DM}(x)$ function as a function of $x$. The comparison of MD results with the value given by equation (16) shows the difference between MGC and MD predictions. MD calculations give a $d_{ex}$ value at ~11 Å ~ 1.2 $\kappa^{-1}$ instead of 16.5 Å ~ 1.9 $\kappa^{-1}$.

Several reasons (not mutually exclusive) could explain the difference in the anion exclusion distance estimated from our MD simulations and the MGC model. The first reason is an inaccuracy of the MD profile due to the low modelled $Cl^-$ concentration associated with an insufficient simulation time. For instance, Figure 5 shows persistent oscillations at distances from the clay surface greater than 20 Å. A second reason could be linked to the MD force field itself. However, this reason is unlikely because (i) Na behaviour is in agreement with MGC predictions and (ii) long range electrostatic interactions are the main contributor to $Cl^-$ distribution. A third reason may be linked to the absence of ion-ion interactions in the MGC model, these interactions taking place in

MD simulation with $Cl^-$ attraction by the plane of $Na^+$ cations. For instance, Carnie and Torrie [49] have shown that MGC models become inaccurate for 1:1 electrolyte at concentrations greater than 0.1 mol $dm^{-3}$ based on Monte-Carlo calculations in similar surface charge conditions. Our simulation conditions would then lie at the limit of applicability of the MGC model. Moreover this result is also supported by the MD data from Marry et al. [17] at 1 mol $L^{-1}$ although their MD simulations were run with a different clay force field [50] to the one used in the present study: an anion exclusion distance of 3.5 Å (~1.2 $\kappa^{-1}$) may be calculated from their data, instead of 5.4 Å from the MGC calculation.

Ideally, the reality of this discrepancy could be tested by comparison with experimental exclusion volume at clay surfaces. Montmorillonite TOT layers are either dispersed or stacked in suspensions. Fully dispersed TOT layers exhibit only "external" surfaces whereas stacked TOT layers exhibit "external" surfaces as well as "internal" surfaces that sandwich interlayer volumes of water considered devoid of anions. As a consequence, measured anion exclusion volumes are due to exclusion from the interlayer volumes and from the diffuse layer volume at external surfaces. The relative ratio of external and internal surface areas must be known to compute the exclusion volume. This ratio can be obtained through knowledge of the average number of TOT-layers in one montmorillonite "particle" ($n_{AV}$). This parameter has been evaluated for Na-montmorillonite, e.g. by light transmission and viscosity ($n_{AV}$ = 1.4 ± 0.4, [51] and references therein) or TEM measurements ($n_{AV}$ = 1.4, [52]). These values point out that most of the Na-montmorillonite TOT layers are dispersed or associated in pairs in dilute suspension. This is further confirmed by the standard deviation value of 0.5 for the average number of platelets as observed by TEM methods ([52]). A ratio $f$ can be defined that is representative of the ratio of TOT layers that are fully dispersed in the

suspension ($0<f<1$, consequently $1-f$ is the ratio of TOT layers that are associated in pairs):

$$n_{AV} = f + (1-f)\times 2 \quad (19)$$

Sposito (1992) has shown that experimental exclusion volume measurements (from [53-56]) can be accurately reproduced for NaCl concentrations less than 0.1 mol $dm^{-3}$ with consideration of exclusion volumes at external and internal surface following:

$$V_{ex} = S_0\left(\frac{d_{ex}}{n_{AV}} + f\frac{d_Q}{2}\right) \quad (20)$$

$S_0$ is the total specific surface area of a single TOT layer of montmorillonite i.e. ~760 $m^2/g$ for a Na-montmorillonite, neglecting the edge surface (5-10 $m^2/g$, [57, 58]). $S$ is the external part of the specific surface area. $d_Q$ is the separation between single-layer platelets in a quasicrystal ($d_Q \sim$ 10Å, [48]).

Equation (20) is almost insensitive to the clay surface charge: a change of charge from -0.125 C $m^{-2}$ to -0.1 C $m^{-2}$ results in volume exclusion differences less than 2%. For the following calculation, the surface charge considered in the present MD study will then be considered (-0.116 C $m^{-2}$). Even if it is clear to us that these data are not sufficient to infirm or confirm the relevance of changing $d_{ex}$ from 1.9 $\kappa^{-1}$ to 1.2 $\kappa^{-1}$ in conditions similar to those simulated in our MD calculations, it may be seen that MD results are in fairly good agreement with the experimental literature data shown in Figure 8.

*4.2.2 Basic Stern parameters derivation from MD concentration profiles*

TLM parameters are the equilibrium constants associated with the surface complexation reactions (at 0 and β-planes), the surface site densities and the capacitances of the inner and outer part of the Stern layer. In the Basic Stern model, only one surface complexation equilibrium constant and the capacitance of the Stern layer are necessary.

The Poisson equation ($\frac{d^2\psi(x)}{dx^2} = -\frac{\rho(x)}{\varepsilon(x)}$, where $\rho$ is the volumetric charge density in C $m^{-3}$), was integrated twice from the bulk water in order to give the value of the potential as a function of the distance from the clay surface ([59]). The result of this double integration depends on the chosen value for $\varepsilon(x)$ in the Stern and diffuse layer. We considered the same permittivity in the diffuse layer as in the bulk water. For the Stern layer ($\varepsilon_{Stern}$) two values were tested: the same permittivity and half the permittivity of the bulk water. From the Na and water MD profile, we initially fixed the end of the "Stern layer" at 6.1 Å from the surface (corresponding to the end of the second water density oscillation). The result of this approach is shown in Figure 9. From $x$ = 0 to $x \sim$ 3.1 Å, the potential is described by a linear increase followed by a "diffuse curve" for $x$ > 3.1 Å. The potential linear increase ($\Delta\psi$) amounts to 85 (from -155 to -70 mV) or 50 mV (from -110 to -60 mV) depending on the considered $\varepsilon_{Stern}$ value, 39.2 and 78.3 respectively. The counter charges accumulation responsible for this potential increase was estimated on the MD profile and corresponds to 0.054 C $m^{-2}$ ($Q_0 = -0.116 + 0.054 = -0.062$ C $m^{-2}$). The description of the interface is consequently well described by a Basic Stern model with a capacitance value of $\frac{-Q_0}{\Delta\psi}$ = 0.73 F $m^{-2}$ for $\varepsilon_{Stern}$ = 39.2 or 1.24 F $m^{-2}$ for $\varepsilon_{Stern}$ = 78.3. The equilibrium constant for Na is accordingly log $K_{Na}$ = 1.64 or 0.88 (see equation (8)). Figure 10 shows the good agreement between calculated Na and Cl concentrations in the diffuse swarm with the Basic Stern model and concentrations simulated with MD. However, with this approach, the diffuse swarm starts in the Na concentration main peak.

*4.2.3 TLM parameters derivation*

Zeta potential is usually considered to be the potential at the top end of the diffuse layer [6, 44]. Zeta potential measurements on montmorillonite are available in the literature at NaCl concentrations comparable to that simulated in the present work (~0.1 mol $L^{-1}$): for instance, Sondi et al. measured a zeta potential of -30 mV at 0.1 mol $L^{-1}$ NaCl with a montmorillonite from Croatia with a CEC of -1.24 $mol_c$ $kg^{-1}$ equivalent to a surface charge of ~-0.16 C $m^{-2}$ [60]. They also showed that the zeta potential remains in the range -40 to -30 mV from $10^{-5}$ to 0.1 mol $L^{-1}$ NaCl. The measurement carried out in the present study led to a zeta potential of -38 mV at 0.12 mol $L^{-1}$ for a montmorillonite with a layer charge of -0.11 C $m^{-2}$. Hence, in our MD experimental conditions the zeta potential value should be between -30 and -40 mV and the top end of the diffuse layer should be at a distance from the surface in-between 5.4 and 7.1 Å (Figure 9) in agreement with the initially considered value (6.1 Å). It should be noted that this result does not depend on the relative permittivity value for the Stern layer (results are almost the same for both values).

The Basic Stern model given above leads to a potential at the top end of the diffuse layer of -70 to -60 mV, clearly in disagreement with the zeta potential measurements. As a consequence, we must either consider (i) that zeta potential is not representative of the potential at the top end of the diffuse layer (in which case, its value cannot be used to parameterize a Basic Stern model as done in [1] or (ii) that the potential is representative of the potential at the top end of the diffuse layer, a more sophisticated model being needed to describe the interface. In the following, a TLM model for the clay surface is proposed.

The 0-plane is located at $x = 0$. The position of the β-plane was fixed by the end of the first linear potential increase at $x_1 = 3.1$ Å from the surface. The charge compensation at the 0-plane, corresponding to equation (6), was estimated with MD concentration

profile from $x$ = 0 to $x$ = 1.6 Å (pre-peak of sodium concentration) and amounts to 0.008 C $m^{-2}$. The charge compensation at the β-plane, corresponding to equation (7), was estimated with MD concentration profile from $x$ = 1.6 to $x$ = 6.1 Å (large peak of sodium concentration) and amounts to 0.076 C $m^{-2}$. The diffuse swarm starts at $x_2 + x_1$ = 6.1 Å, where the potential is -36 mV (Figure 9) in agreement with zeta potential measurements. Considering the potential curve obtained with $\varepsilon_{Stern}$=39.2 in agreement with recent results obtained for oxide surfaces [61], the potential at the 0-plane is -155 mV while the potential at the β-plane is -70 mV. Capacitances $C_1$ and $C_2$ can be calculated accordingly using equations (13) and (14): $C_1$ = 1.27 F $m^{-1}$ and $C_2$ = 0.94 F $m^{-1}$. Note that these values derived from TLM approximation are logically similar to the values that could be directly calculated using the expressions $C_1 = \frac{\varepsilon_{Stern} \times \varepsilon_0}{x_1}$ = 1.12 F $m^{-2}$ and $C_2 = \frac{\varepsilon_{Stern} \times \varepsilon_0}{x_2}$ = 1.13 F $m^{-2}$. The corresponding complexation constants for Na are: log $K_{Na\_0}$ = 2.2 and log $K_{Na\_\beta}$ = -0.23 (see equation (6) and (7)).

It can be seen in Figure 10 that the agreement between simulated with MD and modelled diffuse swarm composition is less accurate with TLM than with the Basic Stern model. However, the potentials at the three planes of interest are accurately reproduced.

## 5. Conclusions

The MGC model captures the essential features of the observations gained from MD simulations made with a 0.1 mol $L^{-1}$ NaCl Na-montmorillonite system i.e. anion exclusion and cation condensation. The MGC model correctly reproduces the Na concentration profile in the diffuse swarm after the Na adsorption "plane". However, we

have shown that the MGC model overestimates anion exclusion by a factor of ~1.5 at ionic strengths above 0.1 mol $L^{-1}$. In addition, our MD simulations made it possible to calculate consistent parameters for the Basic Stern or TLM model (capacitance and sodium complexation constant) with potential applications in cation exchange reaction modelling ([44]) but also in diffusive transport modelling when taking into account the mobility of the exchanged species ([62, 63]).

**Acknowledgments**

This work has been supported by ANDRA (French National Radioactive Waste Management Agency, under the supervision of Dr. S. Altmann), BRGM (French Geological Survey) and the European Commission in the framework of the 6th PCRD Euratom IP FUNMIG. Virginie Marry and Benjamin Rotenberg (LI2C, France) are gratefully acknowledged for their help and suggestions on a first version of this manuscript. The associate editor and the anonymous referee are thanked for their very constructive comments. We are grateful to Dr. Gregory Connelly (Scientific Translations Ltd, France) for proofreading and editing the English text.

## References


[1] M. J. Avena, C. De Pauli, *J. Colloid Interface Sci.* 202 (1998) 195.
[2] P. Leroy, A. Revil, D. Coelho, *J. Colloid Interface Sci.* 296 (2006) 248.
[3] M. Rosanne, N. Mammar, N. Koudina, B. Prunet-Foch, J.-F. Thovert, E. Tevissen, P. M. Adler, *J. Colloid Interface Sci.* 260 (2003) 195.
[4] M. Rosanne, M. Paszkuta, P. M. Adler, *J. Colloid Interface Sci.* 297 (2006) 353.
[5] B. Rotenberg, V. Marry, J. F. Dufreche, N. Malikova, E. Giffaut, P. Turq, *C. R. Chim.* 10 (2007) 1108.
[6] P. Leroy, A. Revil, *J. Colloid Interface Sci.* 270 (2004) 371.
[7] R. O. James, G. A. Parks, *Surf. Colloid Sci.* 12 (1982) 119.
[8] S. Nir, *Soil Sci. Soc. Am. J.* 50 (1986) 52.
[9] S. Nir, D. Hirsch, J. Navrot, A. Banin, *Soil Sci. Soc. Am. J.* 50 (1986) 40.
[10] G. Gouy, *Journal de Physique Théorique Appliquée* 4 (1910) 457.
[11] D. L. Chapman, *Philos. Mag.* 25 (1913).
[12] D. Coelho, M. Shapiro, J. F. Thovert, P. M. Adler, *J. Colloid Interface Sci.* 181 (1996) 169.
[13] S. Levine, G. M. Bell, *Discussions of the Faraday society* 42 (1966) 69.
[14] D. A. Sverjensky, *Geochim. Cosmochim. Acta* 69 (2005) 225.
[15] N. Malikova, A. Cadene, V. Marry, E. Dubois, P. Turq, J.-M. Zanotti, S. Longeville, *Chemical Physics* 317 (2005) 226.
[16] V. Marry, J. F. Dufreche, M. Jardat, G. Meriguet, P. Turq, F. Grun, *Colloids and Surfaces A: Physicochemical and Engineering Aspects* 222 (2003) 147.
[17] V. Marry, B. Rotenberg, P. Turq, *Phys. Chem. Chem. Phys.* 10 (2008) 4802.
[18] N. T. Skipper, F. R. C. Chang, G. Sposito, *Clay. Clay. Miner.* 43 (1995) 285.
[19] N. T. Skipper, P. A. Lock, J. O. Titiloye, J. Swenson, Z. A. Mirza, W. S. Howells, F. Fernandez-Alonso, *Chem. Geol.* 230 (2006) 182.
[20] N. T. Skipper, G. Sposito, F. R. C. Chang, *Clays Clay Miner.* 43 (1995) 294.
[21] J. A. Greathouse, R. T. Cygan, *Environ. Sci. Technol.* 40 (2006) 3865.
[22] B. Rotenberg, V. Marry, J.-F. Dufrêche, E. Giffaut, P. Turq, *J. Colloid Interface Sci.* 309 (2007) 289.
[23] A. Vinsot, S. Mettler, S. Wechner, *Phys. Chem. Earth.* 33 (2008) S75.
[24] A. Pavese, G. Ferraris, M. Prencipe, R. Ibberson, *Eur. J. Miner.* 9 (1997) 1183.
[25] T. Kozaki, A. Fujishima, S. Sato, H. Ohashi, *Nucl. Technol.* 121 (1998) 63.
[26] T. J. Tambach, E. J. M. Hensen, B. Smit, *J. Phys. Chem. B* 108 (2004) 7586.
[27] M. Chavez-Paez, L. dePablo, J. J. dePablo, *The Journal of Chemical Physics* 114 (2001) 10948.
[28] E. C. Gaucher, P. Blanc, F. Bardot, G. Braibant, S. Buschaert, C. Crouzet, A. Gautier, J.-P. Girard, E. Jacquot, A. Lassin, G. Negrel, C. Tournassat, A. Vinsot, S. Altmann, *C.R. Geosci.* 338 (2006) 917.
[29] R. T. Cygan, J.-J. Liang, A. G. Kalinichev, *J. Phys. Chem. B* 108 (2004) 1255.
[30] H. J. C. Berendsen, J. R. Grigera, T. P. Straatsma, *Journal of Physical Chemistry* 91 (1987) 6269.
[31] H. J. C. Berendsen, J. P. M. Postma, W. F. Gunsteren, J. Hermans, *Intermolecular forces*. B. Pullman: Reidel Dordrecht, Holland, 1981.
[32] O. Teleman, B. Jonsson, S. Engstrom, *Mol. Phys.* 60 (1987) 193.
[33] N. Malikova, V. Marry, J.-F. Dufreche, P. Turq, *Current Opinion in Colloid & Interface Science* 9 (2004) 124.

[34] V. Marry, P. Turq, T. Cartailler, D. Levesque, *J. Chem. Phys.* 117 (2002) 3454.
[35] C. D. Schwieters, J. J. Kuszewski, G. M. Clore, *Progress in NMR Spectroscopy* 48 (2006) 47.
[36] C. D. Schwieters, J. J. Kuszewski, N. Tjandra, G. M. Clore, *J. Magn. Reson.* 160 (2003) 66.
[37] L. Kale, R. Skeel, M. Bhandarkar, R. Brunner, A. Gursoy, N. Krawetz, J. Phillips, A. Shinozaki, K. Varadarajan, K. J. Schulten, *J. Comput. Phys.* 151 (1999) 238.
[38] M. Seeber, M. Cecchini, F. Rao, G. Settanni, A. Caflisch, *Bioinformatics* 23 (2007) 2625.
[39] Y. Ichikawa, K. Kawamura, N. Fujii, K. Kitayama, *Applied Clay Science* 26 (2004) 75.
[40] P. Liu, E. Harder, B. J. Berne, *J. Phys. Chem. B* 108 (2004) 6595.
[41] H. Gailhanou, J. C. van Miltenburg, J. Rogez, J. Olives, M. Amouric, E. C. Gaucher, P. Blanc, *Geochim. Cosmochim. Acta* 71 (2007) 5463.
[42] J. C. Rémy, L. Orsini, *Sciences du Sol* 4 (1976) 269.
[43] G. Sposito, *The Surface Chemistry of Natural Particles*. Oxford University Press: New York, 2004; p 242.
[44] P. Leroy, A. Revil, S. Altmann, C. Tournassat, *Geochim. Cosmochim. Acta* 71 (2007) 1087.
[45] J. Wang, A. G. Kalinichev, R. J. Kirkpatrick, *Geochim. Cosmochim. Acta* 70 (2006) 562.
[46] J. Greathouse, G. Sposito, *J. Phys. Chem. B* 102 (1998) 2406.
[47] N. C. Lockhart, *J. Colloid Interface Sci.* 74 (1980) 509.
[48] G. Sposito, in: *Clay-water interface and its rheological implications*, N. Güven; R. M. Pollastro, (Eds.) Clay minerals society: 1992; Vol. 4, pp 127.
[49] S. L. Carnie, G. M. Torrie, *Adv. Chem. Phys.* 56 (1984) 141.
[50] D. E. Smith, *Langmuir* 14 (1998) 5959.
[51] L. L. Schramm, J. C. T. Kwak, *Clay. Clay. Miner.* 30 (1982) 40.
[52] I. Shomer, U. Mingelgrin, *Clays Clay Miner.* 26 (1978) 135.
[53] G. H. Bolt, B. P. Warkentin, *Kolloid Zeitschrift* 156 (1958) 41.
[54] D. G. Edwards, A. M. Posner, J. P. Quirk, *Transactions of the Faraday Society* 61 (1965) 2816.
[55] D. G. Edwards, J. P. Quirk, *Journal of colloid science* 17 (1962).
[56] L. L. Schramm, J. C. T. Kwak, *Colloid. Surface.* 3 (1982) 43.
[57] C. Tournassat, A. Neaman, F. Villiéras, D. Bosbach, L. Charlet, *Am. Mineral.* 88 (2003) 1989.
[58] S. Yokoyama, M. Kuroda, T. Sato, *Clay. Clay. Miner.* 53 (2005) 147.
[59] M. Bostrom, W. Kunz, B. W. Ninham, *Langmuir* 21 (2005) 2619.
[60] I. Sondi, J. Biscan, V. Pravdic, *J. Colloid Interface Sci.* 178 (1996) 514.
[61] T. Hiemstra, W. H. Van Riemsdijk, *J. Colloid Interface Sci.* 301 (2006) 1.
[62] C. A. J. Appelo, A. Vinsot, S. Mettler, S. Wechner, *J. Contam. Hydrol.* 101 (2008) 67.
[63] C. A. J. Appelo, P. Wersin, *Environ. Sci. Technol.* 41 (2007) 5002.

# Tables

Table 1. Scaled diffusion coefficients as a function of the considered (i) force field and (ii) distance from the clay surface.

| | $D_s/D_0$ ($10^{-9}$ $m^2$ $s^{-1}$) | | | | | |
|---|---|---|---|---|---|---|
| | SPC | | | SPC/E | | |
| Zones | $H_2O$ | $Na^+$ | $Cl^-$ | $H_2O$ | $Na^+$ | $Cl^-$ |
| I | 0.24 | 0.21 | | 0.24 | 0.19 | |
| II | 0.34 | 0.05 | | 0.36 | 0.16 | |
| III | 0.31 | 0.46 | | 0.36 | 0.52 | |
| IV | 0.83 | 0.86 | 1.1 | 0.85 | 0.83 | 1 |
| V | 0.98 | 0.96 | 1.1 | 0.97 | 0.91 | 0.9 |
| VI | 1 | 1 | 1 | 1 | 1 | 1 |

# Figure Captions

Figure 1. Sketch of the electrical triple layer model at the clay basal surface in the case of a binary monovalent electrolyte, M represents the metal cations (e.g. $Na^+$) and $A^-$ the anions (e.g. $Cl^-$). OHP represents the Outer Helmholtz Plane (d-plane), which coincides here with the shear plane along which the zeta potential is defined. The β-plane corresponds to the mean plane of the Stern layer while the 0-plane corresponds to the surface of the basal plane. $x_1$: distance from 0-plane to β-plane. Between these two planes, the dielectric permittivity $\varepsilon_1$ applies. $x_2$: distance from β-plane to d-plane. Between these two planes, the dielectric permittivity $\varepsilon_2$ applies. Modified after [44].

Figure 2. Water (top), Na (middle) and Cl (bottom) concentration profiles as a function of the distance from the clay surface. Red line: results obtained with SPC water force field. Blue line: results obtained with SPC/E water force field. Brown lines: coordinates of the most external oxygen atom of the structure. Green lines: coordinates of the most external oxygen atom + ionic radius of oxygen (taken at 1.4 Å). The centre of the system corresponds to the middle of the interlayer. The resolution is 0.5 Å for large figures (mean of 5 ns trajectory) and 0.01 for inserts (mean of 1 ns trajectory).

Figure 3. Na concentration (blue line) and coordination profiles (blue circles, number of water molecules in the first hydration shell taken at 3.2 Å from the Na atoms) as a function of the distance from the centre of the system (mean of 5 ns SPC + 5 ns SPC/E trajectories). Brown line: coordinates of the most external oxygen atom of the structure. Green line: coordinates of the most external oxygen atom + ionic radius of oxygen

(taken at 1.4 Å). The centre of the system corresponds to the middle of the interlayer. The resolution is 0.5 Å for Na concentration and 1 Å for the Na coordination.

Figure 4. Comparison of $D_s(x)/D_0$ of water (blue circles), Na (Na circles) and Cl (green circles) as a function of their distance from the surface of the clay (SPC/E simulations). Lines: water density (blue), Na concentration (red) and Cl concentration (green).

Figure 5. Comparison of Na and Cl concentration profiles obtained from equations (2) to (5) (blue lines) with MD calculations (red lines).

Figure 6. Comparison of Na condensation functions obtained with the MGC model (blue line) and MD calculations (red line). Plain line: with consideration of Na inner-sphere complexes concentration pre-peak. Dotted line: without consideration of Na inner-sphere complexes concentration pre-peak.

Figure 7. Comparison of the anion exclusion distance obtained from MD calculation analysis and the MGC model.

Figure 8. Comparison of experimental chloride exclusion volume at the Na-montmorillonite surface with equation (20) ($n_{AV} = 1.4$) with exclusion distance given by the MGC model (line) or MD simulations (0.12 mol $L^{-1}$: present study and 1 mol $L^{-1}$: [17] ). Data are from [56] (squares and up triangles: experiments at 2 and 4 g montmorillonite $L^{-1}$ respectively), [54] (circles), [55] (diamonds) and [53] (down triangles).

Figure 9. Calculation of the potential $\psi(x)$ as a function of the distance from the clay surface obtained from MD profiles using the integration of the Poisson equation with

two values of relative permittivity for the Stern layer (plain line: 78.3; dotted line: 39.2). Distances of 5.4 and 7.1 Å (drop lines) correspond to potentials of -40 and -30 mV respectively.

Figure 10. Diffuse swarm composition from the Basic Stern model with a capacitance value of 0.73 F $m^{-2}$ (Na: red dashed line; Cl: blue dashed line) and comparison with MD results (Na: red full line; Cl: blue full line). Vertical dotted lines represent the position of the d-plane. Full black line is the water density as a function of the distance from the clay surface.

Figure 11. Diffuse swarm composition from the Triple Layer model with (Na: red dashed line; Cl: blue dashed line) and comparison with MD results (Na: red full line; Cl: blue full line). Vertical dotted lines represent the position of the β and d-planes. The full black line is the water density as a function of the distance from the clay surface.

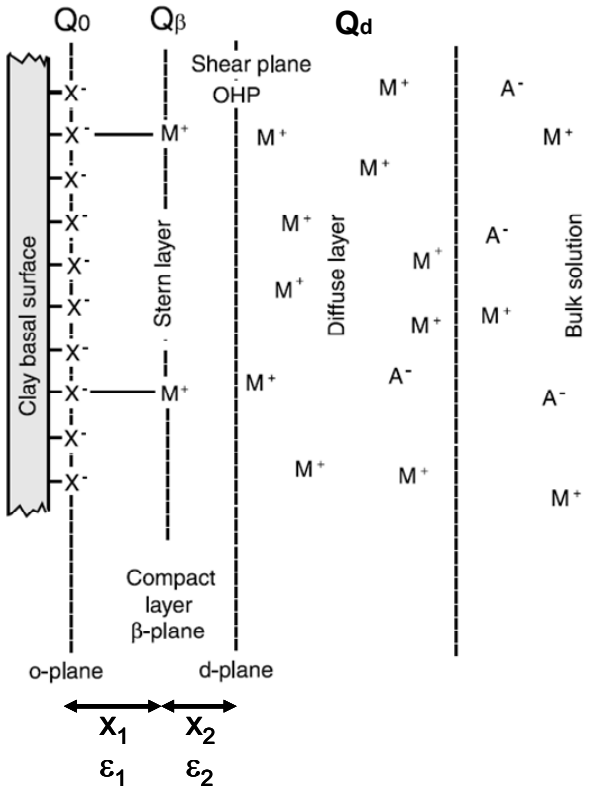


Figure 1. Sketch of the electrical triple layer model at the clay basal surface in the case of a binary monovalent electrolyte, M represents the metal cations (e.g. $Na^+$) and $A^-$ the anions (e.g. $Cl^-$). OHP represents the Outer Helmholtz Plane (d-plane), which coincides here with the shear plane along which the zeta potential is defined. The β-plane corresponds to the mean plane of the Stern layer while the 0-plane corresponds to the surface of the basal plane. $x_1$: distance from 0-plane to β-plane. Between these two planes, the dielectric permittivity $\varepsilon_1$ applies. $x_2$: distance from β-plane to d-plane. Between these two planes, the dielectric permittivity $\varepsilon_2$ applies. Modified after [44].

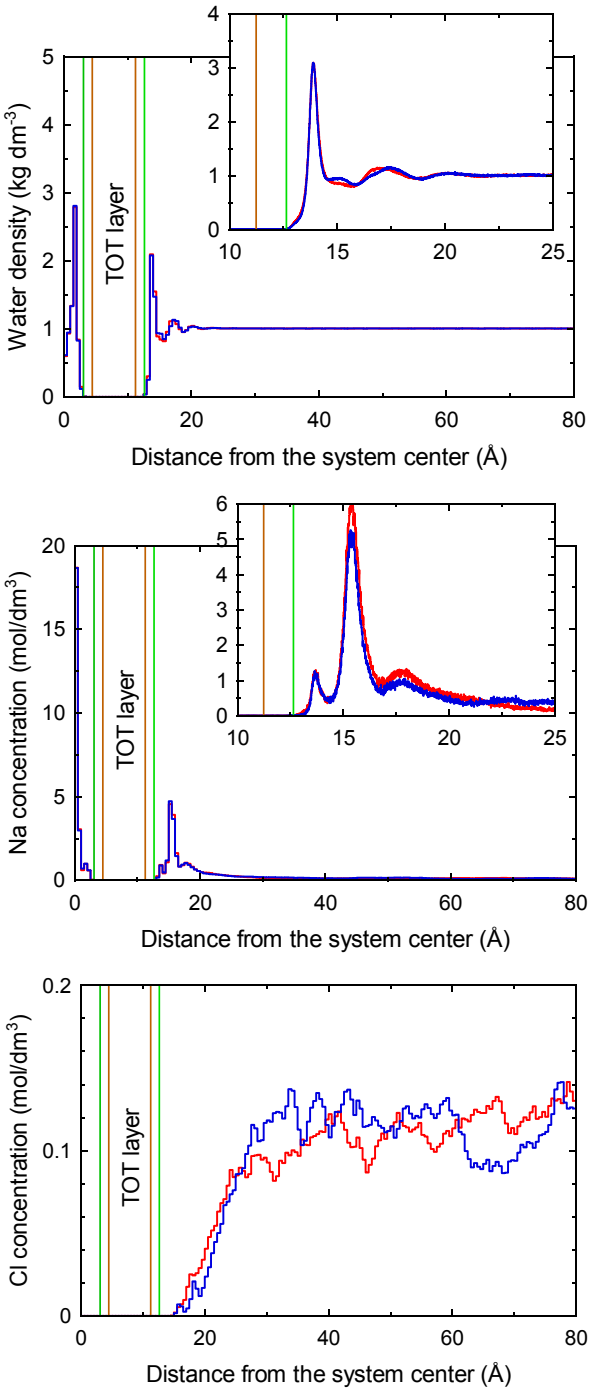


Figure 2. Water (top), Na (middle) and Cl (bottom) concentration profiles as a function of the distance from the clay surface. Red line: results obtained with SPC water force field. Blue line: results obtained with SPC/E water force field. Brown lines: coordinates of the most external oxygen atom of the structure. Green lines: coordinates of the most external oxygen atom + ionic radius of oxygen (taken at 1.4 Å). The centre of the system corresponds to the middle of the interlayer. The resolution is 0.5 Å for large figures (mean of 5 ns trajectory) and 0.01 for inserts (mean of 1 ns trajectory).

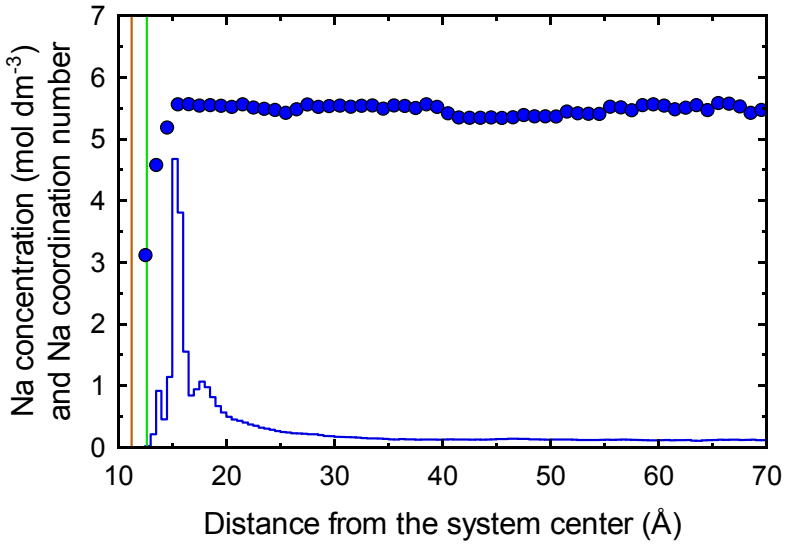


Figure 3. Na concentration (blue line) and coordination profiles (blue circles, number of water molecules in the first hydration shell taken at 3.2 Å from the Na atoms) as a function of the distance from the centre of the system (mean of 5 ns SPC + 5 ns SPC/E trajectories). Brown line: coordinates of the most external oxygen atom of the structure. Green line: coordinates of the most external oxygen atom + ionic radius of oxygen (taken at 1.4 Å). The centre of the system corresponds to the middle of the interlayer. The resolution is 0.5 Å for Na concentration and 1 Å for the Na coordination.

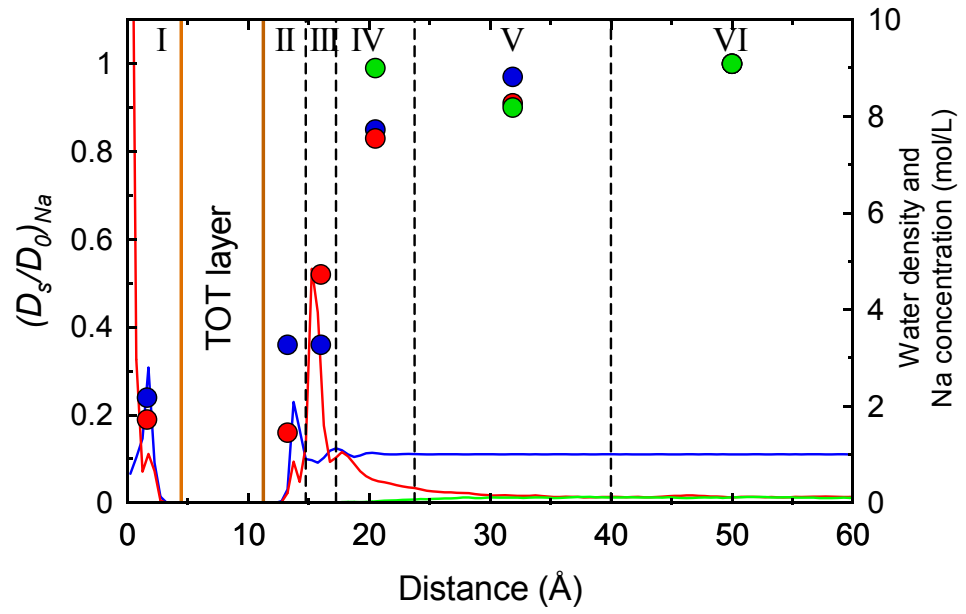


Figure 4. Comparison of $D_s(x)/D_0$ of water (blue circles), Na (Na circles) and Cl (green circles) as a function of their distance from the surface of the clay (SPC/E simulations). Lines: water density (blue), Na concentration (red) and Cl concentration (green).

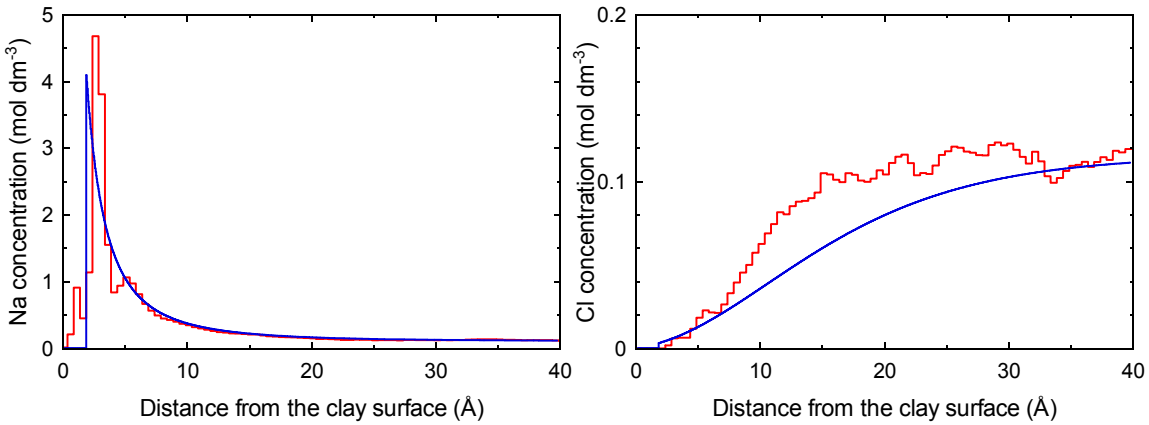


Figure 5. Comparison of Na and Cl concentration profiles obtained from equations (2) to (5) (blue lines) with MD calculations (red lines).

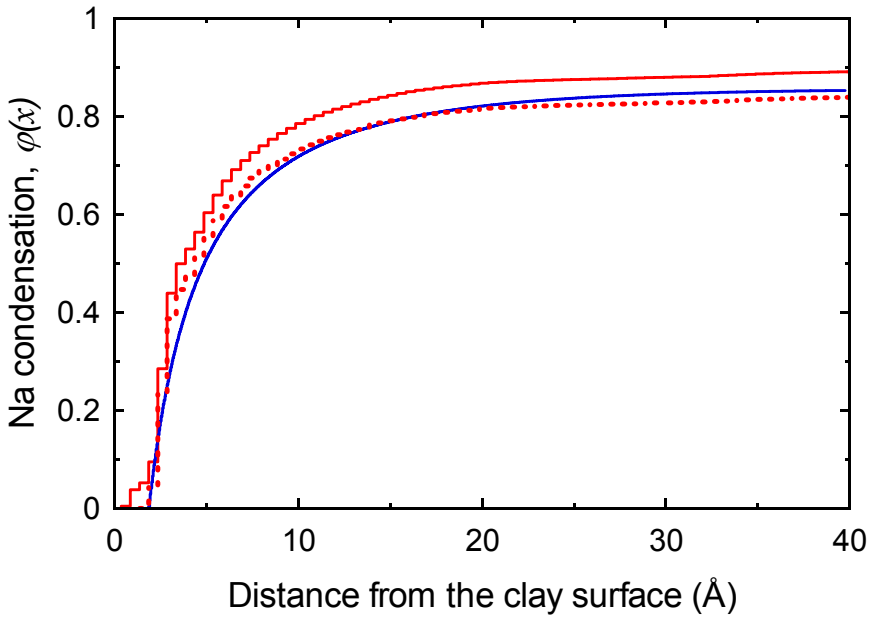


Figure 6. Comparison of Na condensation functions obtained with the MGC model (blue line) and MD calculations (red line). Plain line: with consideration of Na inner-sphere complexes concentration pre-peak. Dotted line: without consideration of Na inner-sphere complexes concentration pre-peak.

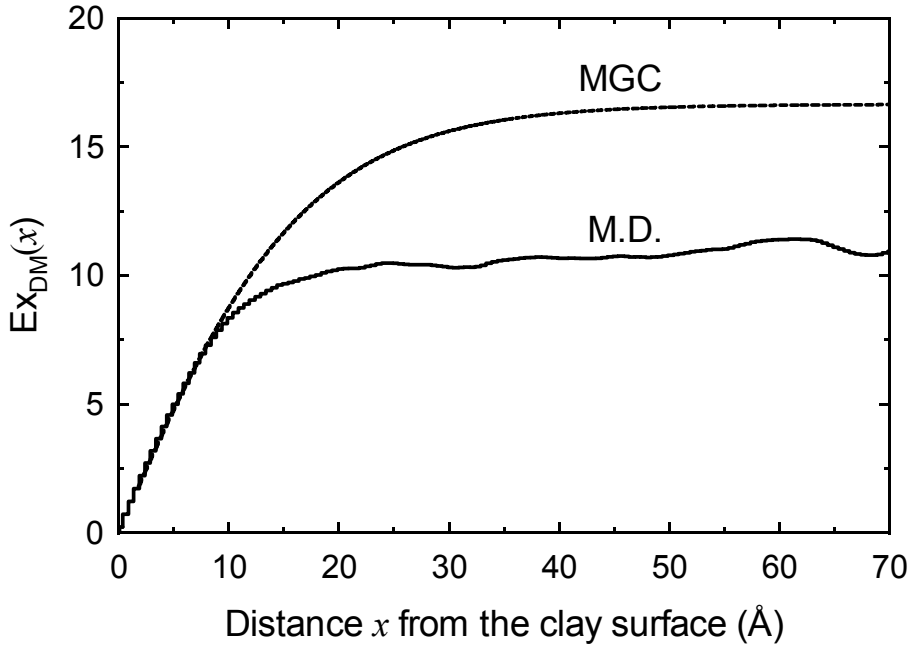


Figure 7. Comparison of the anion exclusion distance obtained from MD calculation analysis and the MGC model.

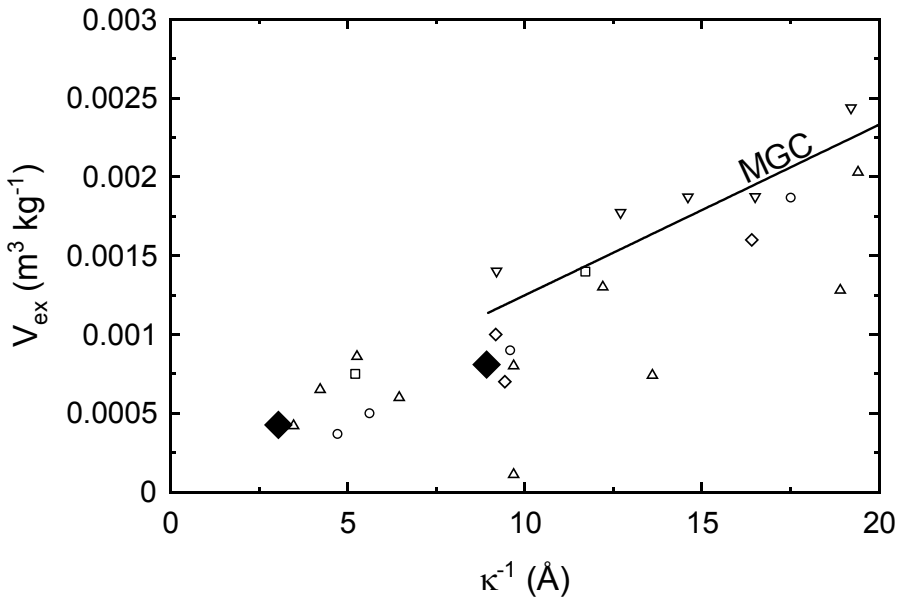


Figure 8. Comparison of experimental chloride exclusion volume at the Na-montmorillonite surface with equation (20) ($n_{AV} = 1.4$) with exclusion distance given by the MGC model (line) or MD simulations (0.12 mol $L^{-1}$: present study and 1 mol $L^{-1}$: [17]). Data are from [56] (squares and up triangles: experiments at 2 and 4 g montmorillonite $L^{-1}$ respectively), [54] (circles), [55] (diamonds) and [53] (down triangles).

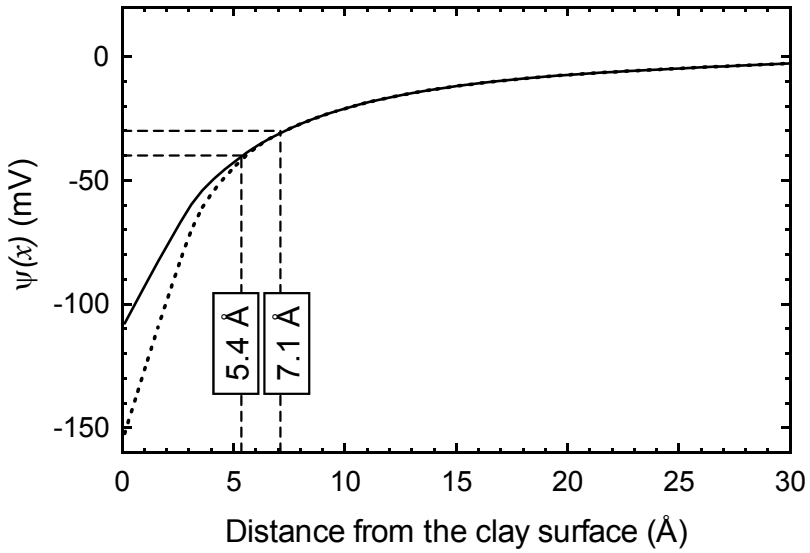


Figure 9. Calculation of the potential $\psi(x)$ as a function of the distance from the clay surface obtained from MD profiles using the integration of the Poisson equation with two values of relative permittivity for the Stern layer (plain line: 78.3; dotted line: 39.2). Distances of 5.4 and 7.1 Å (drop lines) correspond to potentials of -40 and -30 mV respectively.

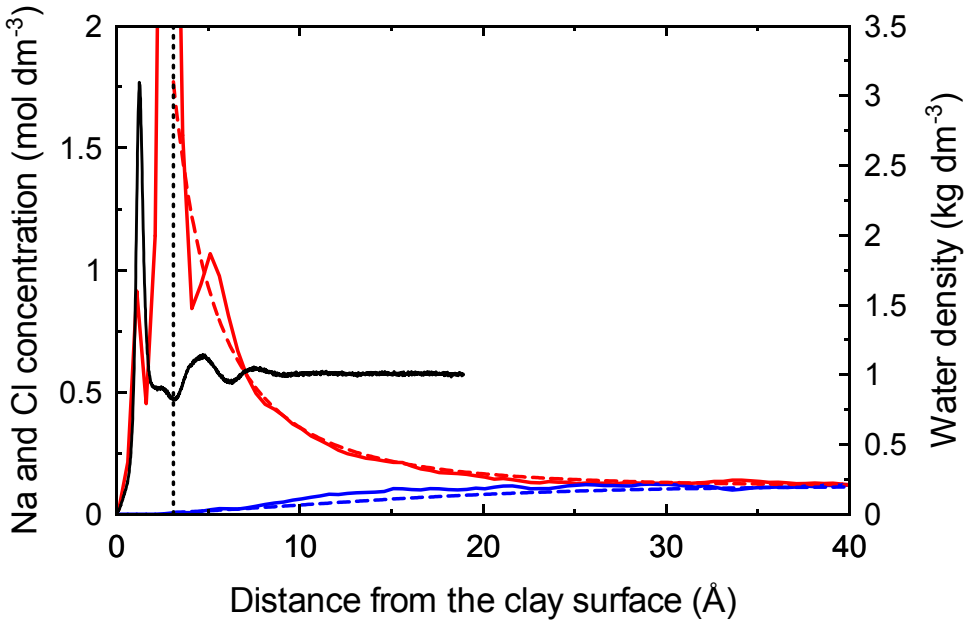


Figure 10. Diffuse swarm composition from the Basic Stern model with a capacitance value of 0.73 F $m^{-2}$ (Na: red dashed line; Cl: blue dashed line) and comparison with MD results (Na: red full line; Cl: blue full line). Vertical dotted lines represent the position of the d-plane. Full black line is the water density as a function of the distance from the clay surface.

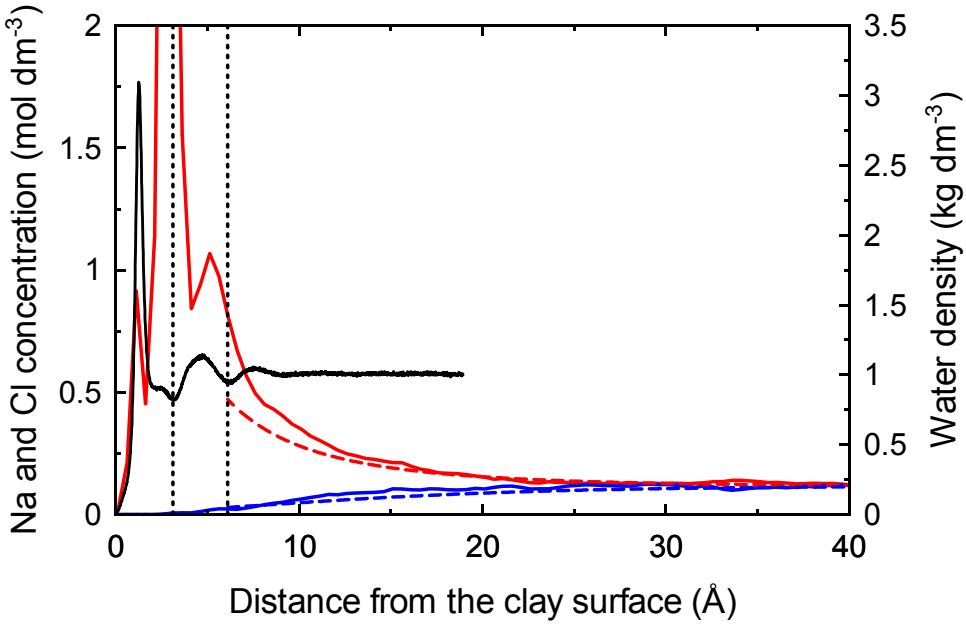


Figure 11. Diffuse swarm composition from the Triple Layer model with (Na: red dashed line; Cl: blue dashed line) and comparison with MD results (Na: red full line; Cl: blue full line). Vertical dotted lines represent the position of the β and d-planes. The full black line is the water density as a function of the distance from the clay surface.